

Strong competition between orbital-ordering and itinerancy in a frustrated spinel vanadate

J. Ma,¹ J. H. Lee,² S. E. Hahn,¹ Tao Hong,¹ H. B. Cao,¹ A. A. Aczel,¹ Z. L. Dun,³ M. B. Stone,¹ W. Tian,¹ Y. Qiu,^{4,5} J. R. D. Copley,⁴ H. D. Zhou,³ R. S. Fishman,^{2,*} and M. Matsuda^{1,†}

¹*Quantum Condensed Matter Division, Oak Ridge National Laboratory, Oak Ridge, Tennessee 37831, USA*

²*Materials Science and Technology Division, Oak Ridge National Laboratory, Oak Ridge, Tennessee, 37831, USA*

³*Department of Physics and Astronomy, University of Tennessee, Knoxville, Tennessee 37996, USA*

⁴*NIST Center for Neutron Research, Gaithersburg, Maryland 20899-6102, USA*

⁵*Department of Materials Science and Engineering,*

University of Maryland, College Park, Maryland 20742, USA

The crossover from localized- to itinerant-electron regimes in the geometrically-frustrated spinel system $\text{Mn}_{1-x}\text{Co}_x\text{V}_2\text{O}_4$ is explored by neutron-scattering measurements and first-principles-guided spin models. At low Co doping, the orbital ordering (OO) of the localized V^{3+} spins suppresses magnetic frustration by triggering a tetragonal distortion. With Co doping, however, electronic itinerancy melts OO and revives the suppressed frustration by weakening the structural and magnetic anisotropies and enhancing the Co-V exchange interactions. Contrary to the predicted chemical-pressure-induced paramagnetism, the measured non-collinear spin states in Co-rich region provide a unique platform where localized spins and electronic itinerancy compete in a geometrically-frustrated spinel.

PACS numbers: 61.05.fm, 75.10.Jm, 75.25.Dk, 75.30.Et

The competition between localized and itinerant behavior triggers many intriguing phenomena such as metal-insulator transitions [1], colossal magnetoresistance [2], and superconductivity in heavy fermion [3] and in Fe-based materials [4]. Likewise, the transformation from itinerant to localized spins in geometrically-frustrated systems creates various exotic phases by modifying the interactions between the spin, orbital, and lattice [5] degrees of freedom. Although the competing effects of localized and itinerant behavior on magnetic frustration have been rather extensively investigated on triangular and pyrochlore lattices, they have been rarely explored on the frustrated spinel AB_2O_4 .

Spinel vanadates are known for their rich phase diagrams produced by the tunable magnetic interactions between the *A* and *B* sites as well as the geometrically-frustrated pyrochlore lattice formed by the *B* sites. Spinel vanadates exhibit additional intriguing characteristics due to the orbital ordering (OO) [6–12] of the partially-filled ($3d^2$) *B*-sites. The competition between OO and itinerancy in the frustrated spinel network may deepen the complexity of the couplings between the magnetic, orbital, and lattice degrees of freedom. However, this complexity also makes it extremely difficult to provide a detailed microscopic understanding of this system [12–17]. Tuning the *A*-site by doping offers the opportunity to systematically study the competition between OO and itinerancy, which strongly interferes with the OO-related transition [6–9, 18]. In particular, the modified spin-orbital-lattice couplings in $\text{Mn}_{1-x}\text{Co}_x\text{V}_2\text{O}_4$ can be used to reveal the competing effects of OO and itinerancy on the coupled magnetic and structural phase transitions [18–20].

We combine elastic and inelastic neutron-scattering

measurements with a first-principles-guided spin-wave model to study single-crystals of $\text{Mn}_{1-x}\text{Co}_x\text{V}_2\text{O}_4$. Contrary to the paramagnetism (para) expected with *A*-site-driven chemical pressure in a Mott-type transition [18], Co doping is found to enhance both the para-to-collinear and collinear-to-noncollinear transition temperatures, T_{CL} and T_{NC} , respectively. Although the magnetic ground state remains a noncollinear ferrimagnet (NC) throughout the entire doping range, this NC state has distinct origins in the localized and itinerant regimes. At low Co doping, OO triggers a coupled cubic-to-tetragonal structural and simultaneous collinear-to-noncollinear magnetic transitions (CL-NC) at $T_S = T_{\text{NC}}$. With higher Co doping, electronic itinerancy decouples the magnetic and structural transitions ($T_{\text{NC}} > T_S$) by melting the OO state. Despite the complete disappearance of OO and of the structural transition, the NC phase is stabilized by the enhanced Co-V exchange at an even higher temperature in the cubic phase derived from all-in/all-out spin structure on the *B*-site pyrochlore lattice. The itinerancy-induced magnetic and structural isotropies revive the magnetic frustration, which produces spin glass behavior and stabilizes novel ground states.

Neutron-diffraction experiments were performed to determine the crystal and magnetic structures using the four-circle diffractometer (HB-3A) and the triple-axis spectrometer (HB-1A) at the High Flux Isotope Reactor (HFIR) of the Oak Ridge National Laboratory (ORNL). The data were refined by the Rietveld method using FULLPROF [21]. Inelastic neutron-scattering (INS) data were collected utilizing both triple-axis and time-of-flight instruments: i) the thermal (HB-1) and cold (CG-

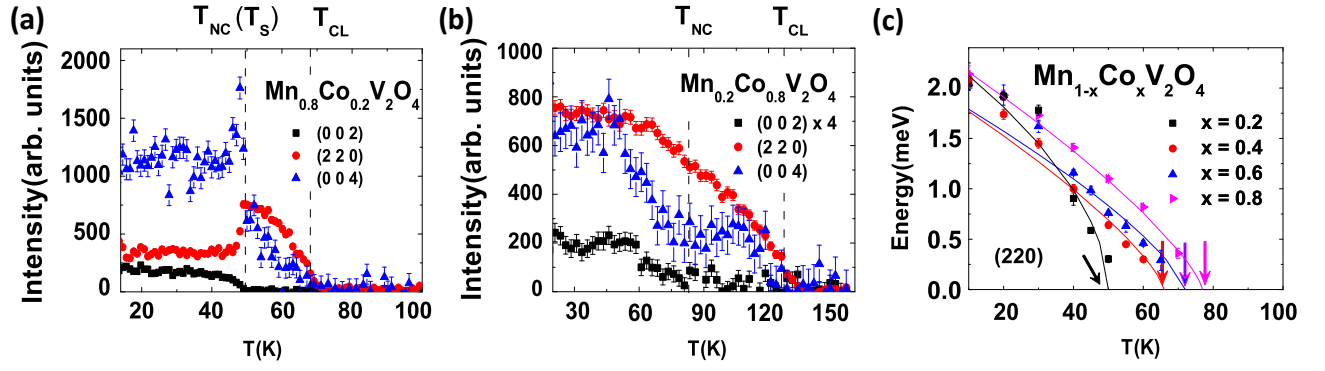


FIG. 1. (color online) Temperature dependence of the Bragg peaks, (002) (squares), (220) (circles), and (004) (triangles) in (a) $\text{Mn}_{0.8}\text{Co}_{0.2}\text{V}_2\text{O}_4$ and (b) $\text{Mn}_{0.2}\text{Co}_{0.8}\text{V}_2\text{O}_4$. (a) and (b) were measured on HB-3A, and the backgrounds are subtracted. (c) Spin-wave energy gap at the magnetic zone center (2,2,0) in $\text{Mn}_{1-x}\text{Co}_x\text{V}_2\text{O}_4$ measured on CG-4C. The lines in (c) are power-law fits. Error bars in the figures represent one standard deviation.

4C) triple-axis spectrometers at HFIR, ORNL, with fixed final energies of 14.7 meV at HB-1 and 5 or 3.5 meV at CG-4C, respectively; ii) the time-of-flight spectrometer, DCS, at National Institute of Standards and Technology (NIST) [22] and SEQUOIA, at the Spallation Neutron Source (SNS) with fixed incident energies of 25.25 and 30 meV, respectively. The data were analyzed by DAVE [23].

Figures 1(a) and (b) show the temperature dependence of the (002), (220), and (004) Bragg peaks for $\text{Mn}_{1-x}\text{Co}_x\text{V}_2\text{O}_4$ ($x=0.2$ and 0.8). At the symmetry-allowed Bragg positions of (220) and (004), the ferromagnetic signals develop below T_{CL} . While the (002) peak is forbidden by symmetry, the observed scattering below T_{NC} indicates the formation of an antiferromagnetic (AFM) spin structure in the ab -plane. The (002) magnetic reflection indicates that the CL-NC magnetic transition at T_{NC} coincides with T_S through $x \approx 0.2$ [10]. For $x = 0.2$, the intensities of the (220) and (004) Bragg peaks rise at ~ 70 K (T_{CL}) due to the para-to-CL magnetic transition, and drop sharply at ~ 50 K ($T_S = T_{NC}$) due to the cubic-to-tetragonal structural transition. For $x > 0.2$, the two transitions become separate with $T_S < T_{NC}$. Although no structural transition is observed at $x = 0.8$, two magnetic transitions are observed with $T_{CL} \sim 150$ K and $T_{NC} \sim 80$ K. X-ray diffraction and heat capacity measurements also suggest the absence of a structural transition in highly Co-doped compounds [20].

In the NC phase below T_{NC} , an easy-axis anisotropy D_{V-V} along the cubic diagonals of each V tetrahedron produces an energy gap in the spin excitation spectrum. Fig. 1(c) presents the spin-wave gap for different temperatures and compositions at the zone center (220). The gap vanishes for the structurally-isotropic cubic CL phase above T_{NC} .

The phase diagram of $\text{Mn}_{1-x}\text{Co}_x\text{V}_2\text{O}_4$ is summarized in Fig. 2. Details are provided in Supplementary Sections

SI and SII. We find for i) $x \leq 0.2$: a para-to-CL magnetic transition at T_{CL} and a cubic-to-tetragonal structural transition that coincides with the CL-NC transition at $T_S = T_{NC} < T_{CL}$; ii) $0.2 < x < 0.8$: the CL-NC and cubic-to-tetragonal transitions are decoupled with $T_S < T_{NC} < T_{CL}$; iii) $x \geq 0.8$: no structural transition is observed down to 5 K but two magnetic phase transitions appear with $T_{NC} < T_{CL}$. Both T_{CL} and T_{NC} increase while T_S gradually decreases with Co^{2+} doping.

In order to analyze the dependence of the magnetic structure and OO on Co doping, we determined the structures of $\text{Mn}_{1-x}\text{Co}_x\text{V}_2\text{O}_4$ ($x=0.0, 0.2$, and 0.8) by single-crystal neutron-diffraction measurement. At low temperatures, the crystal space groups are $I4_1/a$ (tetragonal) for $x=0.0$ and 0.2 and $Fd\bar{3}m$ (cubic) for $x=0.8$. In both unit cells the Mn/Co moments are aligned parallel to the c axis. Above T_{NC} , the V^{3+} moments point along the c axis and antiparallel to the Mn/Co moments. Below T_{NC} , the V^{3+} moments form the two-in/two-out configuration shown in Fig. 2 (b). The canting of the V^{3+} moments away from the c axis starts at 70 K and reaches $22.1(1.8)^\circ$ at 10 K for $x=0.8$, smaller than $35.7(1.5)^\circ$ and $36.2(1.5)^\circ$ for $x=0.0$ and 0.2 at 10 K, respectively. The two-in/two-out structure has been previously observed in MnV_2O_4 [25] and FeV_2O_4 [26].

Although the magnetic state remains NC for all compositions x , the distinct origins of the ground states are illustrated in Fig. 2(b). For low Co-doping, OO of the V ions relieves the magnetic frustration of the pyrochlore lattice and fosters the local two-in/two-out spin state. The Mn-V interactions increase the canting angle while maintaining this two-in/two-out state. However, by inducing itinerancy and fostering isotropic V-V exchange interactions, higher Co doping favors an all-in/all-out spin state. Additional doping also revives the magnetic frustration by weakening the local V anisotropy. Although AFM exchange between the Co and V sites then induces the observed isosymmetric NC spin structure, the

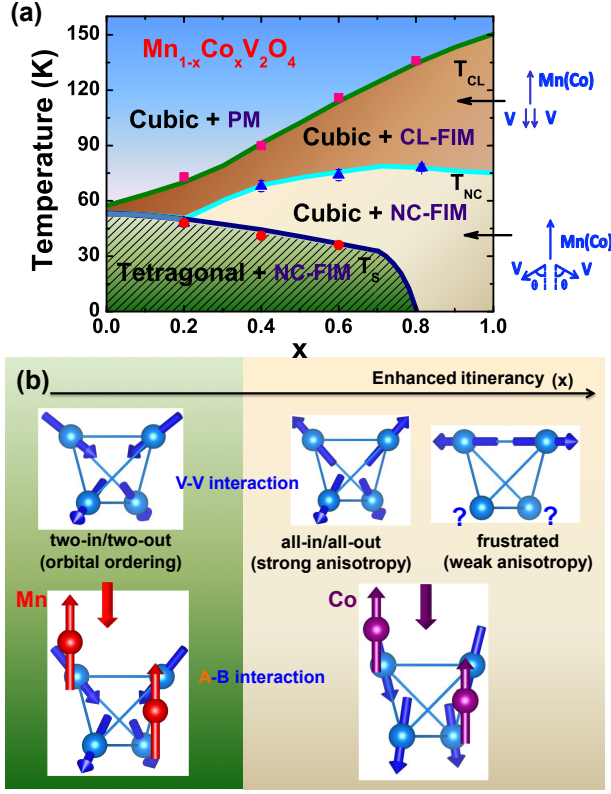


FIG. 2. (color online) (a) The temperature versus Co-doping content (x) phase diagram. The para-to-CL magnetic transition temperature T_{CL} , the CL-NC ferrimagnetic phase transition temperature T_{NC} , and the cubic-to-tetragonal lattice transition temperature T_S are determined from the magnetic susceptibility/heat capacity (solid lines) and neutron-scattering experiments (square, triangle, and circle for the transitions). (b) The hierarchical magnetic states with V-V and V-Mn/Co interactions. The crystal structure was analyzed and visualized using the computer program VESTA [24].

revived frustration is responsible for the measured spin glass behavior [20] due to the alternative states that compete with the two-in/two-out ground state.

The OO state is melted [18] by the electronic itinerancy associated with Co doping. At low temperatures, the V^{3+} ordered moment initially increases from $0.95(4)\mu_B$ ($x=0.0$) to $1.03(7)\mu_B$ ($x=0.2$), then decreases to $0.61(3)\mu_B$ ($x=0.8$). Since the spin and orbital moments are antiparallel at $x=0$, the enhanced V^{3+} moment at $x=0.2$ indicates that the orbital moment is reduced by Co doping. Despite the delocalization of the V^{3+} electrons by chemical pressure, the ordered V magnetic moment does not disappear when $x \geq 0.8$, contrary to the prediction [18] that the smaller Co^{2+} ion ($R_{VV}^{-1}=0.337 \text{ \AA}^{-1}$) triggers paramagnetism.

By combining neutron-scattering measurements with first-principles and model calculations, we find that the strengthened Co-V and isotropic V-V interactions pre-

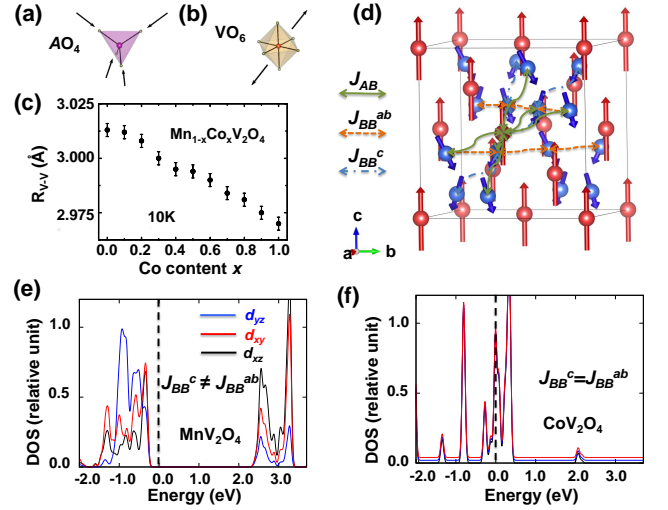


FIG. 3. (color online) (a) AO_4 ($A=Mn^{2+}/Co^{2+}$) tetrahedron and (b) VO_6 octahedron. (c) The x dependence of the $V^{3+}-V^{3+}$ distance, R_{VV} , at 10 K (black dots). (d) NC state of $Mn_{1-x}Co_xV_2O_4$. J_{AB} , J_{BB}^{ab} , and J_{BB}^c are the relative exchange interactions between nearest neighbor of A(B)- and B- site ions. (e) and (f) Density-of-states for AFM MnV_2O_4 and CoV_2O_4 , respectively. Error bars in the figures represent one standard deviation.

serve the V magnetic moment and strengthen the NC state. Strikingly, both T_{CL} and T_{NC} increase with Co doping. In addition to inducing electronic itinerancy, Co-doping also enhances both structural ($c \sim a$) and magnetic isotropy ($J_{BB}^{ab} \sim J_{BB}^c$), as shown in Fig. 3. If the J_{AB} interaction were not also enhanced by Co doping, the remanent magnetic anisotropies along the diagonals of the V tetrahedra would transform the V spin state into an all-in/all-out structure. Due to the enhanced J_{AB} , however, the ground state of the V spins remains in the two-in/two-out state found for small Co doping.

To understand the microscopic effect of Co doping, we consider the structures of the AO_4 tetrahedra and VO_6 octahedra. In the high-temperature cubic phase ($Fd\bar{3}m$), the interior angle of the AO_4 tetrahedra is $\angle O-A-O=109.7^\circ$. With Co doping, the A-O bond length decreases from 2.041 \AA ($x=0$) to 1.984 \AA ($x=0.8$), which applies chemical pressure along the A-O direction as shown in Fig. 3(a). On the other hand, each VO_6 octahedra stretches along the $\langle 111 \rangle$ direction, which produces the local trigonal distortion shown in Fig. 3(b). Due to this distortion, the twelve O-V-O interior angles in the VO_6 octahedra are split away from 90° . With Co^{2+} doping, the difference between the two O-V-O angles decreases from $12.3(2)^\circ$ ($x=0$) to $10.0(2)^\circ$ ($x=0.8$) while the V-O bond length shrinks from $2.023(1) \text{ \AA}$ ($x=0$) to $2.012(1) \text{ \AA}$ ($x=0.8$), which increases both chemical pressure and structural isotropy.

The V-V separation in the V tetrahedra, R_{V-V} , determines both the electronic itinerancy and the related

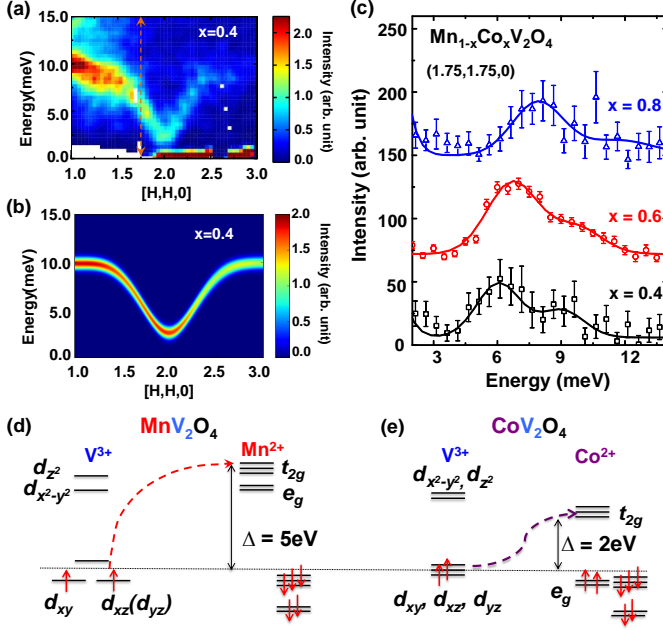


FIG. 4. (color online) (a) and (b) The contour plots of the inelastic neutron scattering intensity in the NC phase of Mn_{0.6}Co_{0.4}V₂O₄ measured at 8 K on SEQUOIA and simulated, respectively. The arrow line (a) represents the position of the constant-Q cut and the white blocks (a) mark the bad detectors. (c) The constant-Q cuts at (1.75, 1.75, 0) in Mn_{1-x}Co_xV₂O₄ measured at 8 K, $x=0.4$ and 0.8 (DCS), and $x=0.6$ (HB-1). The lines in (c) are Gaussian fits and guides to the eye. The low-energy spin-wave branch hardens with Co-doping. (d) and (e) Orbital energies estimated from DFT calculations. Only up-spin energy levels are shown for V³⁺ for simplicity.

lattice structure. At 10 K, R_{V-V} remains almost constant up until $x = 0.2$, above which it begins to decrease. The shorter R_{V-V} increases the bandwidth and induces itinerant electronic behavior, as shown in Fig. 3(e) and (f), thereby suppressing OO. Due to the induced itinerancy and isotropy, T_S falls with Co doping.

The origin of the enhanced J_{AB} is shown in Fig. 4(d), where the orbital energies of both A and B ions are estimated from density-functional theory (DFT). The large energy difference (~ 5 eV) between the occupied V and Mn d states weakens the exchange between Mn and V. By filling the e_g level, Co doping significantly lowers the t_{2g} level and enhances the exchange interaction between Co and V. DFT calculations show that the antiferromagnetic J_{AB} is significantly enhanced in CoV₂O₄ (-2.5 meV) compared to MnV₂O₄ (-1.2 meV). Although the V electrons are delocalized by Co doping, the enhanced J_{A-V} causes T_{CL} to grow. Further, the enhanced magnetic exchange isotropy ($J_{BB}^{ab} \sim J_{BB}^c$) stabilizes the isosymmetric NC phase and raises T_{NC} . Strikingly, induced itinerancy strengthens both the CL and NC phases even without OO.

The spin-wave excitations also provide important information about the magnetic exchanges and anisotropies. Since the interaction between the A^{2+} ions is known to be small [27–29], the interactions between the A^{2+} and V³⁺ ions can be estimated from the dispersion of the observed low-energy acoustic mode. For $x=0.4$, the measured and simulated dispersions along $\langle 110 \rangle$ direction are plotted in Figs. 4(a) and (b). Notice that the spin-wave velocity increases with Co doping, Fig. 4(c). At the magnetic zone center (220), the spin-wave energy gap is plotted as a function of temperature and doping in Fig. 1(c). The gap opens below T_{NC} as the V³⁺ moments cant away from the c axis. Ignoring J_{VV}^{ab} and J_{VV}^c , the spin-wave gap would be proportional to $\sqrt{J_{A-V} \times D_{V-V}}$. We find that a roughly constant spin-wave gap of about 2 meV is maintained by the balance between the increase in J_{A-V} and the decrease in D_{V-V} associated with the itinerancy of the V³⁺ ions.

To summarize, Mn_{1-x}Co_xV₂O₄ exhibits a rich phase diagram due to the crossover from localized to itinerant electronic regimes. The crystallographic and magnetic structures of compounds with low and high Co doping levels have very different physical origins. At low Co doping, OO triggers a cubic-to-tetragonal lattice distortion, accompanied by a CL-to-NC magnetic transition. Co doping contracts R_{V-V} , enhances the electronic itinerancy, and consequently revives the magnetic frustration by weakening the magnetic and structural anisotropies. With further Co doping, OO completely disappears and the magnetic ordering temperatures T_C and T_{NC} are driven higher by the enhanced exchange interaction J_{A-B} . Because CoV₂O₄ is located at the crossover between localized and itinerant electron behavior, external pressure further may strengthen itinerancy and magnetic isotropy, enhance geometric frustration, and produce other exotic behavior. The present results provide a microscopic picture for the competition between OO and electronic itinerancy in the frustrated spinel, and point towards a new methodology for studying competing effects with multiple order parameters.

The research at HFIR and SNS, ORNL, were sponsored by the Scientific User Facilities Division (J.M., S.E.H., T.H., H.B.C., A.A.A., M.S., W.T., M.M.) and Materials Science and Technology Division (J.H.L., R.F.), Office of Basic Energy Sciences, US Department of Energy. S.E.H. acknowledges support by the Laboratory's Director's fund, ORNL. Z.L.D. and H.D.Z. acknowledge the support from JDRD program of University of Tennessee. Work at NIST is supported in part by the National Science Foundation under Agreement No. DMR-0944772. The authors acknowledge valuable discussions with S. Okamoto and G. MacDougall.

REFERENCES

-
- * author to whom correspondences should be addressed:
E-mail:[fishmanrs@ornl.gov]
- † author to whom correspondences should be addressed:
E-mail:[matsudam@ornl.gov]
- [1] M. Imada, A. Fujimori, and Y. Tokura, *Rev. of Mod. Phys.* **70**, 1039 (1998).
 - [2] A. P. Ramirez, *J. Phys.: Condens. Matter* **9**, 8171 (1997).
 - [3] G. R. Stewart, *Rev. of Mod. Phys.* **56**, 755 (1984).
 - [4] Y. Kamihara, H. Hiramatsu, M. Hirano, R. Kawamura, H. Yanagi, T. Kamiya, H. Hosono, *J. Am. Chem. Soc.* **128**, 10012 (2006).
 - [5] C. Lacroix, P. Mendels, and F. Mila, *Introduction to Frustrated Magnetism: Materials, Experiments, Theory*. (Springer, 2001); S. Nakatsuji, Y. Machida, Y. Maeno, T. Tayama, T. Sakakibara, J. van Duijn, L. Balicas, J. N. Millican, R. T. Macaluso, and Julia Y. Chan, *Phys. Rev. Lett.* **96**, 087204 (2006); S. Kumar and J. van den Brink, *Phys. Rev. Lett.* **105**, 216405 (2010) H. Ishizuka and Y. Motome, *Phys. Rev. Lett.* **108**, 257205 (2012); M. Udagawa, H. Ishizuka, and Y. Motome, *Phys. Rev. Lett.* **108**, 066406 (2012); S.-B. Lee, A. Paramekanti, and Y. B. Kim, *Phys. Rev. Lett.* **111**, 196601 (2013).
 - [6] N. Nishiguchi and M. Onoda, *J. Phys. Condens. Matter* **14**, L551 (2002).
 - [7] S. H. Lee, D. Louca, H. Ueda, S. Park, T. J. Sato, M. Isobe, Y. Ueda, S. Rosenkranz, P. Zschack, J. Íñiguez, Y. Qiu, and R. Osborn, *Phys. Rev. Lett.* **93**, 156407 (2004).
 - [8] E. M. Wheeler, B. Lake, A. T. M. N. Islam, M. Reehuis, P. Steffens, T. Guidi, and A. H. Hill, *Phys. Rev. B* **82**, 140406(R) (2010).
 - [9] A. Kismarhardja, J. S. Brooks, H. D. Zhou, E. S. Choi, K. Matsubayashi, and Y. Uwatoko, *Phys. Rev. B* **87**, 054432 (2013).
 - [10] V. O. Garlea, R. Jin, D. Mandrus, B. Roessli, Q. Huang, M. Miller, A. J. Schultz, and S. E. Nagler, *Phys. Rev. Lett.* **100**, 066404 (2008).
 - [11] G. J. MacDougall, I. Brodsky, A. A. Aczel, V. O. Garlea, G. E. Granroth, A. D. Christianson, T. Hong, H. D. Zhou, and S. E. Nagler, *arXiv* 1403.0269, (2014).
 - [12] T. Katsufuji, T. Suzuki, H. Takei, M. Shingu, K. Kato, K. Osaka, M. Takata, H. Sagayama, and T.-H. Arima, *J. Phys. Soc. Jpn.* **77**, 053708 (2008).
 - [13] S. Di Matteo, G. Jackeli, and N. B. Perkins, *Phys. Rev. B* **72**, 020408(R) (2005).
 - [14] H. Tsunetsugu, and Y. Motome, *Phys. Rev. B* **68**, 060405(R) (2003).
 - [15] Gia-Wei Chern, Natalia Perkins, and Zhihao Hao, *Phys. Rev. B* **81**, 125127 (2010).
 - [16] S. Sarkar, T. Maitra, Roser Valentí, and T. Saha-Dasgupta, *Phys. Rev. Lett.* **102**, 216405 (2009).
 - [17] K. Myung-Whun, S. Y. Jang, T. Katsufuji, and A. V. Boris, *Phys. Rev. B* **85**, 224423 (2012).
 - [18] S. Blanco-Canosa, F. Rivadulla, V. Pardo, D. Baldomir, J.-S. Zhou, M. García-Hernández, M. A. López-Quintela, J. Rivas, and J. B. Goodenough, *Phys. Rev. Lett.* **99**, 187201 (2007).
 - [19] A. Kismarhardja, J. S. Brooks, A. Kiswandhi, K. Matsubayashi, R. Yamanaka, Y. Uwatoko, J. Whalen, T. Siegrist, and H. D. Zhou, *Phys. Rev. Lett.* **106**, 056602 (2011).
 - [20] A. Kiswandhi, J. S. Brooks, J. Lu, J. Whalen, T. Siegrist, and H. D. Zhou, *Phys. Rev. B* **84**, 205138 (2011).
 - [21] J. Rodriguez-Carvajal, Recent advances in magnetic structure determination by neutron powder diffraction. *Physica B* **192**, 55 (1993).
 - [22] J. R. D. Copley and J. C. Cook, *Chem. Phys.* **292**, 477 (2003).
 - [23] R. T. Azuah, L. R. Kneller, Y. Qiu, P. L. W. Tregenna-Piggott, C. M. Brown, J. R. D. Copley, and R. M. Dimeo, *J. Res. Natl. Inst. Stan. Technol.* **114**, 341 (2009).
 - [24] K. Momma and F. Izumi, *J. Appl. Crystallogr.*, **44**, 1272 (2011).
 - [25] A. J. Magee, *Spin correlations in frustrated magnets with orbital ordering* Ch. 4 (Ph.D. thesis, Royal Holloway, University of London 2010).
 - [26] G. J. MacDougall, V. O. Garlea, A. A. Aczel, H. D. Zhou, and S.E. Nagler, *Phys. Rev. B* **86**, 060414(R) (2012).
 - [27] R. Nanguneri and S. Y. Savrasov, *Phys. Rev. B* **86**, 085138 (2012).
 - [28] T. Suzuki, M. Katsumura, K. Taniguchi, T. Arima, and T. Katsufuji, *Phys. Rev. Lett.* **98**, 127203 (2007).
 - [29] J.-H. Chung, J.-H. Kim, S.-H. Lee, T. J. Sato, T. Suzuki, M. Katsumura, and T. Katsufuji, *Phys. Rev. B* **77**, 054412 (2008).